CSIRO PUBLISHING

COLLECTION | RESEARCH PAPER
https://doi.org/10.1071/WF25161

International Journal of WILDLAND FIRE
International Association of Wildland Fire

Probabilistic prediction of post-fire debris-flow runout and implications for prefire assessments of post-fire hazards

Alexander N. Gorr[A,*], Luke A. McGuire[A], Ann M. Youberg[B] and Donald N. Lindsay[C]

For full list of author affiliations and declarations see end of paper

***Correspondence to:**
Alexander N. Gorr
The University of Arizona, Department of Geosciences, Gould-Simpson Building, 1040 East Fourth Street, Tucson, AZ 85721, USA
Email: agorr@arizona.edu

Received: 1 July 2025
Accepted: 7 January 2026
Published: 9 February 2026

Cite this: Gorr AN *et al.* (2026) Probabilistic prediction of post-fire debris-flow runout and implications for prefire assessments of post-fire hazards. *International Journal of Wildland Fire* **35**, WF25161. doi:10.1071/WF25161

ABSTRACT

Background. Debris-flow runout modeling is a valuable component of the prefire assessment of post-fire hazards. The application and benefits of runout modeling are limited by uncertainty in debris-flow volume as well as model parameters related to flow mobility. **Aims.** In this study, we assess and reduce the uncertainty associated with flow-mobility parameters by calibrating a debris-flow runout model to 12 runoff-generated debris flows in the western United States. **Methods.** For each debris flow, we determined optimal flow-mobility parameters using back analyses and generated a posterior distribution of the parameters using a Bayesian approach. We assessed the relative sensitivity of the model to the flow-mobility parameters, rainfall intensification and fire burn severity when applied to three post-fire debris flows. **Key results.** Yield strength, one of the flow-mobility parameters, exhibits a negative, linear relationship with soil clay content. Modeled area inundated is most sensitive to the flow-mobility parameters, followed by a rainfall intensification factor. **Conclusions.** Well-constrained flow-mobility parameters will improve post-fire debris-flow runout modeling, though prefire assessments of post-fire hazards could also benefit from accounting for the effects of rainfall intensification. **Implications.** This study improves our ability to simulate debris-flow runout and assess associated hazards.

Keywords: area inundated, Bayesian analysis, debris flow, fire, hazard, inundation, modeling, rainfall intensification, runout, soil clay content.

Introduction

Debris flows often occur following fire owing to increases in infiltration-excess overland flow and erosion in steep watersheds in response to short-duration, high-intensity rainfall (Kean *et al.* 2011; Nyman *et al.* 2011; McGuire *et al.* 2024). Although post-fire debris flows (PFDFs) already pose a hazard to people and infrastructure downstream of fire-prone regions around the world (Conedera *et al.* 2003; García-Ruiz *et al.* 2013; Nyman *et al.* 2015; Kean *et al.* 2019; Jin *et al.* 2022; Esposito *et al.* 2023), climate-driven increases in fire activity (Senande-Rivera *et al.* 2022), intensification of short-duration rainfall (Fowler *et al.* 2021) and expansion of the wildland–urban interface (Radeloff *et al.* 2018) could exacerbate PFDF hazards in the coming decades (Kean and Staley 2021; Thomas *et al.* 2024). Simulating debris-flow runout before a fire occurs, especially using methods that incorporate uncertainty in poorly constrained parameters, can help identify areas at risk from future PFDFs.

Parameters that influence flow mobility in debris-flow runout simulations are often constrained through back-analyses of past events, particularly with equivalent fluid models that represent debris flows as an idealized fluid (Hürlimann *et al.* 2008; Aaron *et al.* 2019; Zimmermann *et al.* 2020). However, guidance to aid with parameter selection specifically for runoff-generated debris flows that tend to initiate in recently burned areas is limited. Thus, information about past events and the corresponding optimal flow-

Collection: Establishing Directions in Post-fire Debris-Flow Science

mobility parameters can assist with forward model analyses by providing guidance on reasonable parameter ranges. Calibration to past events can also provide guidance for simulating events in similar settings (Aaron *et al.* 2022) and reveal relationships between model parameters and flow constituents (Zimmermann *et al.* 2020) that can inform parameter selection in forward analyses.

Calibrating flow-mobility parameters can yield estimates of a single set, or a distribution, of optimal parameters (Aaron *et al.* 2019). A single set of optimal flow-mobility parameters can be obtained by maximizing an objective function that quantifies the degree of similarity between a modeled quantity and a set of observations (Heiser *et al.* 2017). A drawback to this approach is that a range of parameter choices can yield similar model outcomes and selection of a single set of optimal parameters fails to account for uncertainty in the observations used to assess model performance. An alternative method for calibrating runout models is to employ a Bayesian approach that accounts for uncertainty in debris-flow runout observations (Aaron *et al.* 2019). The outcome of this type of model calibration is a probability distribution over the model parameters, referred to as the posterior distribution, that quantifies how consistent a given set of flow-mobility parameters is with prior beliefs and observed data. The posterior distribution can inform input parameter sets for forward model analyses, including probabilistic predictions of debris-flow runout (Aaron *et al.* 2022; Liu *et al.* 2024).

In cases where runout model parameters can be constrained, time limitations can still make it challenging to incorporate debris-flow runout modeling into rapid post-fire hazard assessments. Steep landscapes are most susceptible to runoff-generated PFDFs in the immediate aftermath of a fire, as approximately 23% of PFDFs start in the first 60 days after a fire start date and 73% start in the first post-fire year (McGuire *et al.* 2024). Prefire assessments of post-fire hazards that include estimates of debris-flow runout can help prioritize watersheds for prefire treatments and identify downstream areas for debris-flow mitigation measures to reduce risks before a fire (Rossi *et al.* 2025).

In addition to constraints on flow-mobility parameters, debris-flow runout simulations require estimates of flow volume. Existing methods for predicting PFDF volume have found that volume depends on terrain, fire and rainfall characteristics (e.g. Gartner *et al.* 2008, 2014; Gorr *et al.* 2024*a*). Thus, within the context of a prefire assessment of post-fire hazards for a given watershed, debris-flow volume will be influenced by burn severity and rainfall intensity. Burn severity in prefire assessments can be derived from models (Staley *et al.* 2018; Wells *et al.* 2023) or assigned based on different scenarios of interest, and the rainfall intensity of design storms can be determined from historical rainfall records (e.g. NOAA Atlas 14). Rainfall intensification, however, is likely to increase sub-hourly rainfall intensities in the future (Martel *et al.* 2021), which may lead to increases in debris-flow likelihood and volume in response to a storm with a given recurrence interval (Thomas *et al.* 2024). As prefire assessments of PFDF hazards aim to identify risks following a fire at some unknown time in the future, there are benefits to exploring the influence of rainfall intensification relative to other sources of uncertainty, such as that associated with flow-mobility parameters, on modeled runout.

The objectives of this study are to (1) constrain flow-mobility parameters for a debris-flow runout model, the Progressive Debris-Flow routing and inundation model (ProDF) (Gorr *et al.* 2022), through back-analyses of 12 debris-flow events, and (2) use a detailed analysis of three of these debris flows to assess the sensitivity of modeled inundation area to flow-mobility parameters, a rainfall intensification factor constrained by climate model output and a burn severity factor. Accomplishing these objectives will improve our ability to conduct prefire assessments of PFDF runout.

Study areas

We compiled inundation data from 10 runoff-generated PFDFs and 2 runoff-generated debris flows that started in unburned areas across nine study sites in the western United States (US) (Fig. 1, Table 1). The properties of the debris flows included in this inundation dataset, as well as the watersheds that produced them, vary widely. The 12 debris-flow-producing watersheds included in this study range in size from 0.2 to 31.4 km^2, with a median area of 3.2 km^2 (Table 1). The mean elevation of the watersheds ranges from 605 m above mean sea level (amsl) to 2971 m amsl. Debris-flow volume varies from 1000 to 304,000 m^3, with a median volume of 38,500 m^3, and the area inundated by the flows ranges from 1600 to 1,534,000 m^2, with a median area of 68,600 m^2 (Table 1). Some of the debris flows ran out onto fans where the potential for flow confinement was minimal, whereas others were more confined and emptied into larger channels downstream.

The characteristics of the study sites themselves also vary considerably, so we separated the sites into three geographic regions: southern California, northern California and the Southwest (Table 1).

Southern California

Our dataset includes four PFDFs from two study sites in southern California, one that initiated following the 2016 Fish Fire and another three that initiated following the 2017 Thomas Fire (Fig. 1, Table 1). Both study sites, which are located in the Transverse Ranges, are dominated by chaparral and oak woodlands at lower elevations and coniferous forests at higher elevations and are characterized by a Mediterranean climate (Griffith *et al.* 2016). Most precipitation in the region falls between November and March, often in the form of long-duration storms called atmospheric rivers (Lamjiri *et al.* 2018).

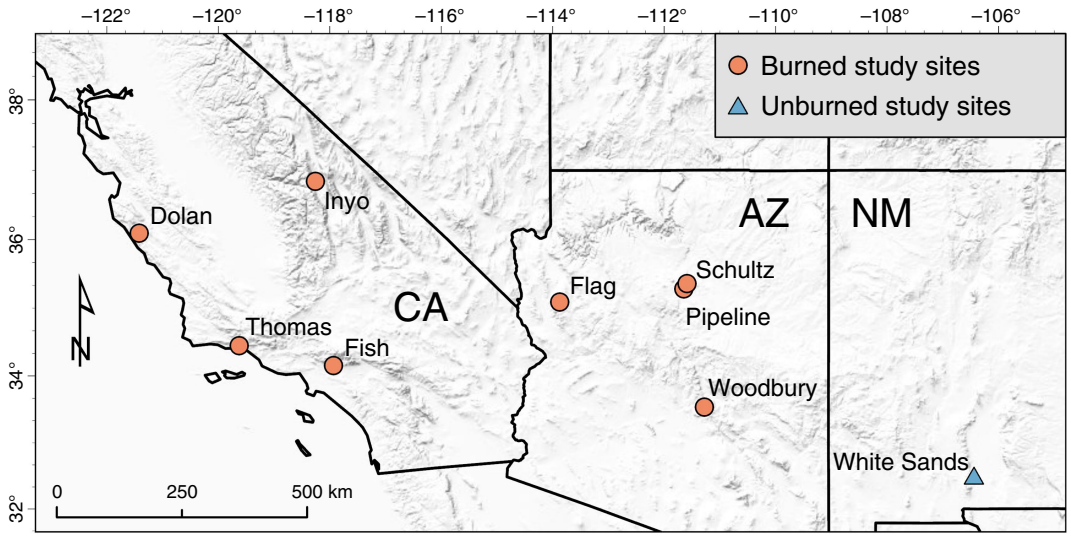

Fig. 1. This study includes inundation data from 12 runoff-generated debris flows that initiated at nine study sites across Arizona (AZ), California (CA) and New Mexico (NM) in the western United States. Ten of the debris flows initiated following wildfire and the remaining two started in unburned settings. We separated the study sites into three geographic regions: northern California (Dolan and Inyo), southern California (Fish and Thomas) and the Southwest (Flag, Pipeline, Schultz, White Sands and Woodbury).

Table 1. Site characteristics for all 12 debris flows.

Study site	Debris flow	Region	Mean annual temperature (°C)[A]	Mean annual precipitation (mm)[A]	Watershed area (km^2)	Inundated area (m^2)
Dolan Fire	Santa Lucia Creek	Northern California	14.5	923	3.9	45,200
Fish Fire	Van Tassel	Southern California	17.8	644	2.5	55,600
Flag Fire	Solitude	Southwest	11.7	407	0.2	3300
Inyo Complex	Oak Creek	Northern California	5.1	469	31.4	1,045,100
Pipeline Fire	Copeland	Southwest	5.6	813	1.1	518,200
Schultz Fire	Basin 5210	Southwest	5.6	813	0.7	32,300
Thomas Fire	Buena Vista/ Romero Creeks	Southern California	16.6	692	6.9	926,700
Thomas Fire	Montecito Creek	Southern California	16.8	625	12.3	1,292,300
Thomas Fire	Oak/San Ysidro Creeks	Southern California	16.8	666	8.5	1,534,000
Woodbury Fire	B7	Southwest	19.9	400	0.2	1600
White Sands Missile Range[B]	Black Mountain	Southwest	15.6	319	0.5	24,500
White Sands Missile Range[B]	Kent Peak	Southwest	16.6	286	4.5	81,600

[A]Data from PRISM Climate Group (2025).
[B]Unburned study site.

Northern California

Our dataset also includes PFDFs from two study sites in northern California. One debris flow initiated following the 2007 Inyo Complex and another initiated following the 2020 Dolan Fire (Fig. 1). The Inyo Complex site is located in the Sierra Nevada and has extensive coniferous forest cover (Griffith *et al.* 2016). The Dolan Fire site is located in the coastal mountains of central California and is dominated by grassland, shrubland and woody savannas (Thomas *et al.* 2023). The northern California sites are characterized by hot, dry summers and moist, cool winters

(Wilken *et al.* 2011) and much of the winter precipitation comes in the form of atmospheric rivers (Lamjiri *et al.* 2018).

The Southwest

The remaining six debris flows occurred at five study sites in the Southwest US, defined here as the states of Arizona and New Mexico. Four are PFDFs that initiated following the 2010 Schultz Fire, 2019 Woodbury Fire, 2021 Flag Fire and 2022 Pipeline Fire, and the other two are non-fire-related debris flows that initiated in the White Sands Missile Range of southern New Mexico following intense rainfall in 2021 (Fig. 1, Table 1). Although the White Sands Missile Range debris flows initiated in an unburned setting, they had a similar initiation mechanism to the PFDFs in this study, so we included them in our analysis to create a larger inundation dataset. Dominant vegetation community varies by site, from desert scrub and shrub communities at lower elevation (Woodbury Fire and White Sands Missile Range), to ponderosa pine (*Pinus ponderosa*) and mixed-conifer forests at higher elevation (Flag Fire, Schultz Fire and Pipeline Fire) (Wilken *et al.* 2011). Climatologically, the Southwest is characterized by warm to hot summers, mild winters and low mean annual precipitation, particularly at lower elevations (Wilken *et al.* 2011). Unlike California, approximately half of the annual precipitation in the Southwest falls during the summer as short-duration, high-intensity rainfall associated with the North American monsoon (Sheppard *et al.* 2002).

Methods

Debris-flow runout modeling

We used ProDF, a reduced-complexity debris-flow runout model based on a flow-routing algorithm (Gorr *et al.* 2022), to simulate the runout of all 12 debris flows. ProDF can be used to compute peak-flow depth across a landscape based on topography and flow volume. The model equations include flow density (kg/m^3), as well as two flow-mobility parameters, referred to as the flow resistance coefficient (χ) (1/s m$^{1/2}$) and yield strength (τ) (Pa).

ProDF simulates peak debris-flow depth and velocity downstream of a user-specified location, or 'starting point', where a debris-flow volume is known or estimated (for more detailed description, see Gorr *et al.* 2022). Inputs for ProDF include topography, the location of the starting point, debris-flow volume and values for density, χ and τ. We utilized high spatial-resolution, pre-event topography for 11 of the 12 debris flows. However, because there was no high-resolution, pre-event topography available for the Schultz Fire site (Table 1), we used post-event topography collected 8 years following the debris flow. For consistency across sites, we used 3 m input topography for all simulations.

The starting point for a ProDF simulation is defined as the location where the model begins routing the flow downstream. In this study, we defined the starting point for all debris flows as the watershed outlet. This is consistent with the input debris-flow volumes used here, which represent the volume of sediment deposited downstream of the watershed outlet. We used previously published volume data for eight debris flows (Youberg 2015; Kean *et al.* 2019; McGuire *et al.* 2021; Morelan 2021; Gorr *et al.* 2023, 2024*b*) and calculated the volume of the four remaining debris flows using a combination of field surveys, remote sensing techniques and empirical modeling (Supplementary material Text S1).

We fixed the density parameter to 2000 kg/m^3 for all simulations because ProDF is not sensitive to density relative to χ and τ (Gorr *et al.* 2022). However, because the model is sensitive to the flow mobility parameters (Gorr *et al.* 2022), we assessed the performance of ProDF against each debris flow using a range of χ and τ values. We considered χ values between 0 and 1500 1/s m$^{1/2}$ (Rickenmann 1999) and τ values between 0 and 3000 Pa (e.g. Major and Pierson 1992; Whipple and Dunne 1992). We determined the best-performing values of χ and τ for each debris flow by calibrating ProDF to the observed inundation extent using two calibration methods described in more detail below. The inundation data we used to calibrate ProDF consisted of both previously published maps of debris-flow inundation (Youberg 2015; Kean *et al.* 2019; Morelan 2021; Gorr *et al.* 2023, 2024*b*) and new inundation data we collected using a combination of field surveys and remote sensing techniques (Supplementary Text S2).

Model calibration

Conventional calibration

We performed a conventional calibration of the two flow-mobility parameters, χ and τ, for all 12 debris flows using the method outlined in Gorr *et al.* (2022). In short, we calibrated χ and τ to minimize the misfit between the modeled and observed inundation extent. We first generated 30,000 unique combinations of χ and τ within the ranges defined earlier using the Latin hypercube sampling method (McKay *et al.* 1979). We then ran 30,000 simulations of ProDF, one for each unique combination of χ and τ, for each debris flow.

We quantified model performance using the similarity index (Ω_T) (Heiser *et al.* 2017; Gorr *et al.* 2022), which quantifies the misfit between the modeled and observed inundation extent using the number of true positive (TP) points (modeled and mapped inundation overlap), false positive (FP) points (modeled inundation but no mapped inundation) and false negative (FN) points (mapped inundation but no modeled inundation). The similarity index is defined as:

$$\Omega_T = \alpha_T - \beta_T - \gamma_T$$

where α_T, defined as TP/(TP + FP + FN), represents the overlap between the modeled and mapped inundation, β_T, defined as FN/(TP + FP + FN), represents areas of model

underestimation, and γ_T, defined as FP/(TP + FP + FN), represents areas of model overestimation. The value of Ω_T varies between 1 and −1, where 1 indicates a perfect fit between the modeled and mapped inundation and −1 represents a total misfit. We calculated the similarity index for all 30,000 combinations of χ and τ for each debris flow and identified the best-performing combination as the one that yielded the highest similarity index.

Bayesian parameter estimation

We also calibrated ProDF using a Bayesian parameter estimation method. This approach uses a likelihood function to combine prior information about the flow-mobility parameters with information from observed data to produce a posterior distribution, which represents the uncertainty in the parameters after they have been updated based on their ability to reproduce the observed inundation extent of a debris flow. The posterior distribution quantifies the probability that a given pair of χ and τ minimizes the difference between the modeled and observed inundation extent. The posterior distribution of χ and τ values obtained using the Bayesian approach can then be used in a probabilistic forward analysis (Aaron *et al.* 2019).

We simulated the area inundated by each debris flow using the same 30,000 combinations of χ and τ used for the conventional calibration. We then used the trimline fitness metric, hereafter referred to as fitness (Aaron *et al.* 2019), to quantify how well each combination reproduced the mapped extent of inundation for each scenario. The fitness for a given combination of χ and τ can be defined as (Liu *et al.* 2024):

$$\text{fitness} = \text{FP} + \text{FN}$$

A smaller fitness value indicates a better fit between the modeled and observed extent of inundation, with zero representing a perfect fit. Then, following the methodology of Aaron *et al.* (2019), we used the fitness values to calculate the posterior distribution.

In addition to determining the posterior distribution, we calculated the 50% credible region for each debris flow. A credible region, defined as the area within a posterior distribution that contains a specified probability mass (in this case 0.5) provides a way to summarize uncertainty associated with the calibrated flow-mobility parameters. To determine the 50% credible region, we sorted the probability values for each combination of χ and τ in descending order. We then summed the probability values of the parameter combinations, starting with the highest probability and incorporating sequentially smaller values, until the total probability exceeded 50%.

Finally, to summarize the posterior distributions, we calculated the mean values of χ and τ for each debris flow, referred to as the expected values. We did so by multiplying each value of χ and τ by their corresponding probability and summing the products. We then calculated the variance by taking the average of the squared deviations from the expected values, where each deviation was weighted by its corresponding probability in the distribution.

Controls on flow-mobility parameters

To explore potential controls on the flow-mobility parameters, we analyzed the relationships between debris-flow volume, watershed average soil clay content and the optimal flow-mobility parameters. For this analysis, we utilized the optimal sets of parameter values identified from the conventional calibration as well as the expected values from the posterior distributions of χ and τ from the Bayesian calibration. We computed Spearman correlation coefficients (ρ) to quantify the strength of the relationship between each of the two flow-mobility parameters and debris-flow volume and watershed soil clay content. We focused on flow volume and soil clay content because previous studies found that both are related to debris-flow mobility. For instance, Iverson (1997) determined that deeper debris flows, which are associated with greater flow volumes (Rickenmann 1999), tend to be more mobile because they retain elevated pore-fluid pressures longer than thinner flows. Similarly, the fines content of debris flows, which includes clay content, influences pore-fluid pressure, and thus flow mobility (Iverson 1997; de Haas *et al.* 2015). Previous studies have also found that debris-flow volume is related to area inundated, indicating that larger debris flows are more mobile and have the potential to impact greater areas downstream (Corominas 1996; Griswold and Iverson 2008).

We used the Stream Catchment (StreamCat) Dataset (Hill *et al.* 2016) to determine the mean soil clay content for each watershed. StreamCat separates the conterminous US into more than 2.5 million individual watersheds and provides watershed-scale data related to climate, lithology, land cover and soil properties (Hill *et al.* 2016). It uses data from the State Soil Geographic (STATSGO) database (Schwarz and Alexander 1995) to determine the clay content for each watershed within its dataset. Although the STATSGO database provides separate clay content values for each layer within a soil profile, StreamCat records the mean clay content within a watershed.

Sensitivity analysis

We conducted an analysis to quantify model sensitivity to the flow-mobility parameters, rainfall intensification under future climate scenarios and burn severity. Quantifying the relative sensitivity to these different factors can provide guidance on where to focus future efforts aimed at reducing uncertainty in prefire assessments of PFDF hazards. For this analysis, we selected three debris flows that spanned a range of geographic regions and dominant vegetation types: Copeland in northern Arizona, Montecito Creek in southern California and Santa Lucia Creek in northern California (Table 1).

Numerical experiments

We set up simulations at the three selected sites to represent debris-flow inundation in response to a 2-year recurrence interval (RI) 15-min rainfall intensity. We selected a 2-year RI rainstorm because it is broadly representative of storms that are associated with most PFDFs in the western US (Staley *et al.* 2020; McGuire *et al.* 2024; Martinez *et al.* 2025). We determined debris-flow volumes for a given rainfall intensity using the Emergency Assessment Volume (EAV) model of Gartner *et al.* (2014). The EAV model predicts post-fire debris-flow volume as a function of the peak 15-min rainfall intensity ($i15$), watershed relief (R) and the area burned at moderate to high severity (A_{mh}).

We varied $i15$ between a minimum value, taken as the 2-year RI rainstorm, and a maximum value based on a rainfall intensification factor designed to account for future changes in rainfall intensity–duration–frequency curves (Martel *et al.* 2021). We used NOAA Atlas 14 to determine 15-min rainfall intensity associated with the 2-year RI rainstorm at each site. We then determined the maximum potential value of $i15$ by multiplying the 2-year RI rainstorm by a rainfall intensification factor (Martel *et al.* 2021):

$$i15_f = i15_h(100 + R_{sc}/100)^{\Delta T}$$

where ΔT denotes the projected change in local mean annual temperature (°C) between the historical period (1950–2014) and a future time period and R_{sc} is a rainfall scaling factor (%) based on the Clausius–Clapeyron (CC) relation. The CC relation suggests $R_{sc} = 7\%$; however, because rainfall intensities associated with shorter duration events (i.e. sub-hourly) can follow a super CC relationship (Fowler *et al.* 2021) and the 15-min rainfall intensity is an input to the EAV model, we used $R_{sc} = 8\%$. We estimated ΔT at each of our sites based on projected temperature changes between historical and mid- (2045–2074) or late- (2075–2100) century under a range of Shared Socioeconomic Pathways (SSP) climate scenarios, specifically SSP2-4.5, SSP3-7.0 and SSP5-8.5. The SSP5-8.5 scenario represents a worst-case high emissions scenario, SSP3-7.0 is the second highest emissions scenario and SSP2-4.5 is a moderate emissions scenario.

We extracted temperature changes for each site from LOCA2, which is a statistically downscaled 6 km gridded product (Pierce *et al.* 2023). LOCA2 includes estimates of minimum and maximum monthly temperature for mid- and late-century for SSP2-4.5, SSP3-7.0 and SSP5-8.5 from 27 Coupled Model Intercomparison Project Phase 6 (CMIP6) models. We averaged the minimum and maximum temperatures in each of the six scenarios to determine a mean annual temperature. We then took the difference of this mean annual temperature and the historical average to determine ΔT for each of the models. We used the median of the resulting 27 values for $i15_f$ to define a representative rainfall scaling factor, γ, for each climate scenario.

We performed 1000 debris-flow runout simulations for each of the six climate scenarios (i.e. mid- and late-century for SSP2-4.5, SSP3-7.0 and SSP5-8.5) at each case study location. We sampled flow-mobility parameters from the posterior distribution using a probability proportional to size sampling approach (Skinner 2016). We sampled the $i15$ associated with a 2-year RI rainstorm from a uniform distribution bounded by $i15$ and $\gamma i15$. We defined the area burned at moderate to high severity as cA, where A is watershed area (km^2) and c, the burn severity factor, was sampled from a uniform distribution between 0.2 and 1. The rainfall intensification factor and burn severity factor influence runout through their effects on flow volume as computed by the EAV model.

We defined the area inundated as the area that experienced peak-flow depths greater than 0.1 m. We used the PAWN sensitivity index (Pianosi and Wagener 2015) to assess the relative importance of different factors in determining inundated area. The PAWN sensitivity index varies from 0 to 1, with a greater value indicating greater parameter importance. The goal of these numerical experiments was to assess the relative importance of the flow-mobility parameters, rainfall scaling factor and burn severity factor for each of the six different climate scenarios. We also assessed the importance of each variable relative to a dummy parameter, which had no effect on the model output and was sampled from a uniform distribution between 0 and 1. Variables with a PAWN sensitivity index that is similar to or less than that of the dummy are not influential.

Results

Optimal parameter sets

Using the conventional calibration methods, we determined an optimal combination of χ and τ for each of the 12 debris flows. The optimal value of the flow resistance coefficient (χ) ranged from approximately 5 to 250 1/s m$^{1/2}$ but was between 5 and 50 1/s m$^{1/2}$ for 75% (9 of 12) of debris flows. The optimal value of yield strength (τ) varied from ~200 to 1800 Pa but was less than 800 Pa for 66% (8 of 12) of debris flows (Table 2). These optimal parameter combinations yielded similarity index (Ω_T) values between −0.18 and 0.59, with a median of 0.07. There was a significant negative relationship between the optimal τ value for all 12 debris flows and watershed clay content (C) ($\rho = -0.76$, $P = 0.004$) (Fig. 2). The relationship between C and τ can be represented by a line, $\tau = 2900 - 129C$ ($R^2 = 0.78$) (Fig. 3*a*). We also found a moderate, but not statistically significant, negative relationship between τ and debris-flow volume ($\rho = -0.50$, $P = 0.10$). In contrast, there was no substantial correlation between either C and χ ($\rho = 0.14$, $P = 0.66$) or debris-flow volume and χ ($\rho = -0.28$, $P = 0.38$) (Fig. 2). We observed similar relationships

Table 2. Optimal flow-mobility parameters and associated similarity index for each debris flow.

Study site	Debris flow	χ (1/s m$^{1/2}$)	τ (Pa)	Ω_T	Volume (m^3)	Clay content (%)
Dolan Fire	Santa Lucia Creek	4.5	1514	0.29	23,000	13.4
Fish Fire	Van Tassel	47.8	416	0.59	38,613	18.5
Flag Fire	Solitude	46.4	878	-0.02	1100	17.2
Inyo Complex	Oak Creek	42.9	355	0.08	304,000	7.5
Pipeline Fire	Copeland	108	193	-0.14	115,000	21.4
Schultz Fire	Basin 5210	70.6	251	-0.02	15,000	21.4
Thomas Fire	Buena Vista/Romero Creeks	24.1	232	-0.18	141,000	21.7
Thomas Fire	Montecito Creek	20.5	297	0.14	231,000	18.2
Thomas Fire	Oak/San Ysidro Creeks	15.1	298	0.20	307,000	18.8
Woodbury Fire	B7	36.7	1140	0.06	1000	12.6
White Sands Missile Range	Black Mountain	30.9	1775	0.19	22,000	18.0
White Sands Missile Range	Kent Peak	256	333	0.01	38,500	18.0

when we removed the two non-fire-related debris flows from the White Sands Missile Range from our analysis (Supplementary Table S1), suggesting that ProDF performed similarly in both burned and unburned settings.

Although there were some strong relationships between the optimal flow-mobility parameters and site-specific characteristics, regional-scale patterns in optimal values for χ and τ were less apparent. At the two northern California sites, the optimal χ values ranged from 4.5 to 42.9 1/s m$^{1/2}$, nearly a factor of 10 (Table 2), and the optimal τ values varied by approximately a factor of 5, from 355 to 1514 Pa (Table 2). We observed a similarly large spread in the optimal flow-mobility parameters for the six Southwest debris flows, where optimal χ values varied from 30.9 to 256 1/s m$^{1/2}$, and optimal τ values ranged from 193 to 1775 Pa (Table 2). There was, however, considerably less variation in the optimal flow-mobility parameters among the four southern California debris flows, as the optimal χ values varied between 15.1 and 47.8 1/s m$^{1/2}$ and the optimal τ values ranged from 232 to 416 Pa (Table 2).

Bayesian calibration

Using the Bayesian parameter estimation calibration method, we generated posterior distributions for all 12 debris flows. Relationships between C, flow volume and the expected values of χ and τ obtained from the posterior distributions (Table 3) were similar to the relationships observed using the conventional calibration. One exception is that there was no substantial correlation between τ and flow volume (Supplementary Fig. S1) when using the expected values of χ and τ. The strongest relationship was still between C and τ, which can be represented by the line $\tau = 1413 - 55C$ ($R^2 = 0.81$) (Fig. 3*b*).

To summarize uncertainty associated with the calibrated flow-mobility parameters, we calculated the 50% credible regions for each debris flow. All twelve 50% credible regions plot, at least partly, in the lower-left quadrant of the parameter space (Fig. 4). Each study region, however, plots in its own parameter space with little overlap. For example, the 50% credible regions for the four southern California debris flows were more tightly grouped relative to the 50% credible regions of the other eight debris flows across northern California and the Southwest (Fig. 4). This observation is supported by the fact that the expected χ and τ values for the southern California debris flows were much more similar than those of the other eight debris flows (Table 3).

The size of the 50% credible regions (larger credible regions indicate greater uncertainty) (Fig. 4) and the variance of the posterior distributions (Table 3) provide insights into factors that influence uncertainty in calibrated flow-mobility parameters. We found a large disparity in the average size of the 50% credible region depending on geographic region (Fig. 4*a*). The 50% credible regions for the four southern California debris flows (Fig. 4*b*) contained 44 combinations of the flow-mobility parameters, on average, and the 50% credible regions for the eight debris flows outside of southern California (Fig. 4*c*, *d*) contained 233 combinations of χ and τ, on average. The five debris flows with the largest 50% credible regions were located in the Southwest, and the debris flows with the greatest spread in χ and τ values were located in the Southwest and northern California (Fig. 4). This is consistent with the observation that posterior distributions for χ and τ in the Southwest and Northern California regions had median variances that were approximately 24 times and 4 times greater, respectively, than the median variances of the posterior distributions for χ and τ in southern California (Table 3).

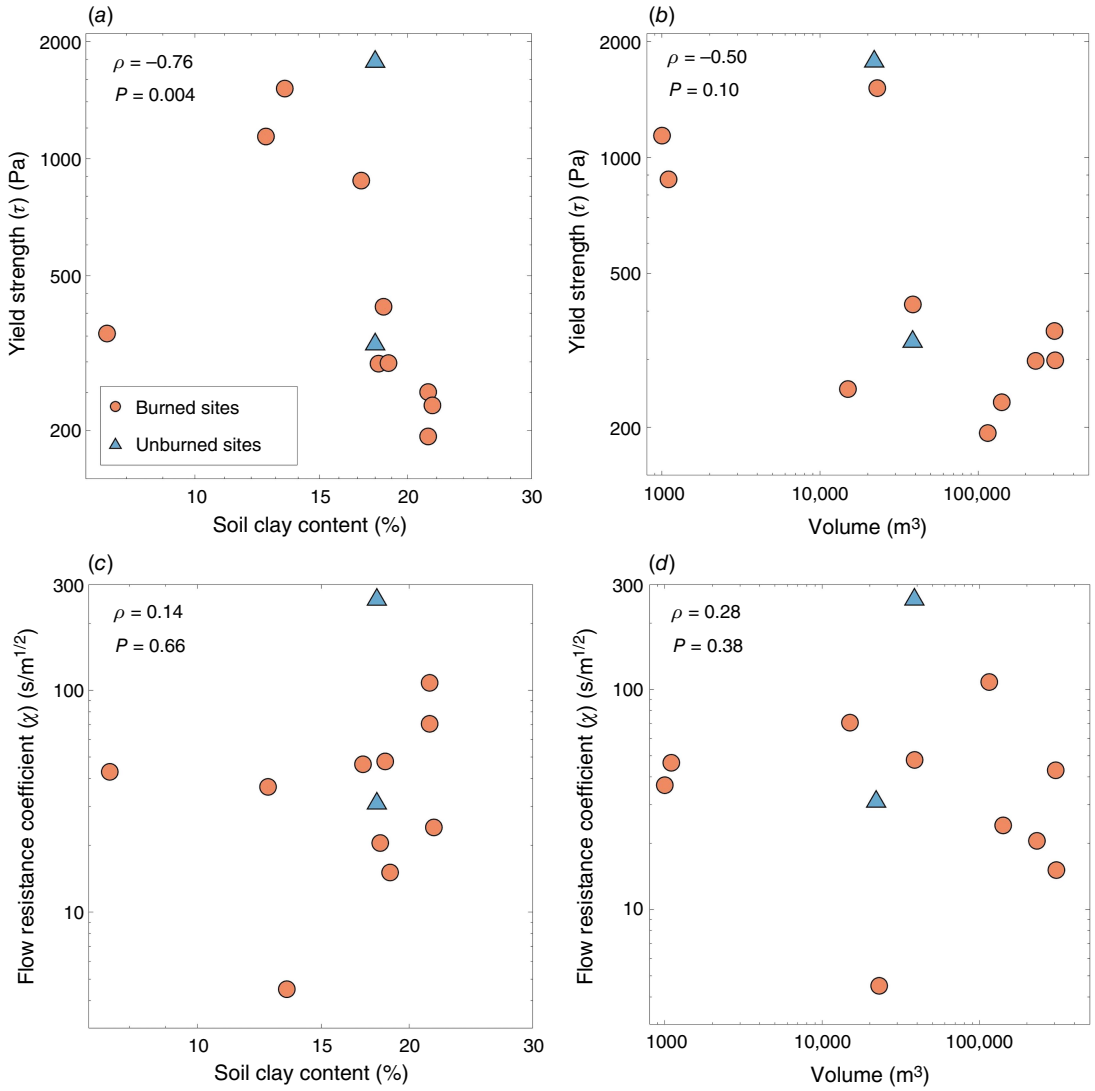

Fig. 2. Relationships between yield strength, determined from the conventional calibration, and (*a*) soil clay content, and (*b*) flow volume. The Spearman correlation coefficient, ρ, indicates a negative and statistically significant correlation between yield strength and clay content. There is no statistically significant correlation between the flow resistance coefficient and (*c*) soil clay content, or (*d*) flow volume.

We also found that the size of the 50% credible region generally decreased with increasing debris-flow volume. The 50% credible regions for seven debris flows with volumes less than 100,000 m^3 contained 225 combinations of χ and τ, on average, and the 50% credible regions for five debris flows with volumes larger than 100,000 m^3 contained 93 combinations of the flow-mobility parameters, on average. The variance in χ and τ was lower, in general, when flow volume exceeded 100,000 m^3 relative to cases where volume was less than 100,000 m^3 (Table 3).

Sensitivity analysis

The flow resistance coefficient (χ) was the most influential parameter for determining area inundated in 15 of 18 cases (three sites, six climate scenarios), and it had a greater influence on area inundated relative to τ at all three sites (Fig. 5). The area inundated at the Copeland and Santa Lucia Creek sites was most sensitive to χ, regardless of climate scenario (Figs 5a, *b*), but the relative importance of different parameters varied depending on the climate scenario at the Montecito Creek site. At this site, area inundated was most sensitive to either χ, the rainfall intensification factor, or the burn severity factor depending on the climate scenario (Fig. 5*c*).

The rainfall intensification factor was more influential than the dummy variable at all sites regardless of the climate scenario but became increasingly influential in late-century SSP3-7.0 and SSP5-8.5 scenarios. The rainfall intensification factor was more influential relative to the

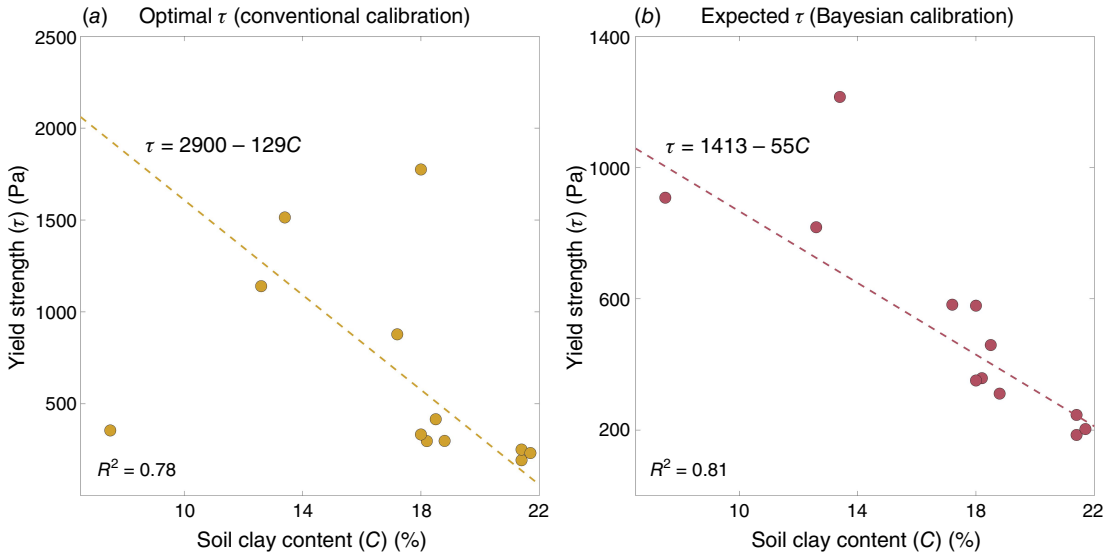

Fig. 3. Best fit lines quantifying the relationship between clay content, *C*, and (*a*) the optimal yield strength, τ, identified through the convention calibration, and (*b*) the expected (mean) yield strength based on the posterior distribution obtained through the Bayesian calibration.

Table 3. Expected (mean) χ and τ values determined through the Bayesian parameter estimation and associated variance for all 12 debris flows.

Study site	Debris flow	Region	Expected χ (1/s m$^{1/2}$)	Expected τ (Pa)	χ variance	τ variance
Dolan Fire	Santa Lucia Creek	Northern California	14.1	1215	238	210,593
Fish Fire	Van Tassel	Southern California	71.1	459	3,329	27,788
Flag Fire	Solitude	Southwest	191	582	33,848	76,023
Inyo Complex	Oak Creek	Northern California	45.0	908	1488	428,320
Pipeline Fire	Copeland	Southwest	428	185	65,848	16,198
Schultz Fire	Basin 5210	Southwest	148	246	26,217	10,113
Thomas Fire	Buena Vista/Romero Creeks	Southern California	191	203	68,002	52,406
Thomas Fire	Montecito Creek	Southern California	29.9	358	338	24,835
Thomas Fire	Oak/San Ysidro Creeks	Southern California	22.3	311	260	11,279
Woodbury Fire	B7	Southwest	182	818	53,012	120,031
White Sands Missile Range	Black Mountain	Southwest	349	579	83,188	213,471
White Sands Missile Range	Kent Peak	Southwest	515	351	76,259	22,615

burn-severity factor in all late-century (2075–2100) SSP3-7.0 and SSP5-8.5 scenarios except for the SSP3-7.0 scenario at Montecito Creek. The burn-severity factor was more influential relative to the rainfall intensification factor at all three sites for early- and late-century SSP2-4.5 scenarios (Fig. 5).

Discussion

Controls on flow-mobility parameters

These results provide guidance for selecting flow-mobility parameters for runoff-generated PFDFs in the absence of a

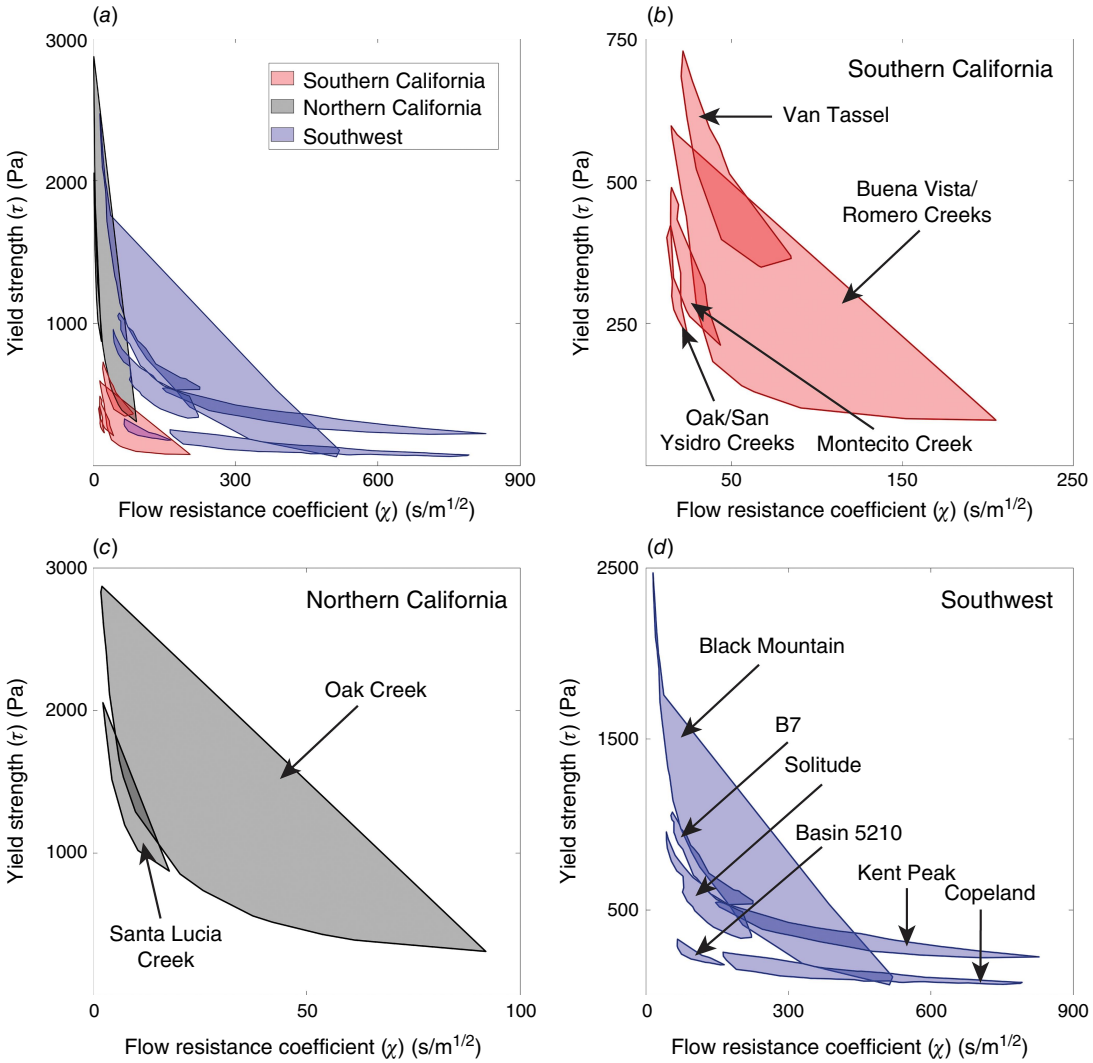

Fig. 4. The 50% credible regions for (*a*) all 12 debris flows, (*b*) four southern California debris flows, (*c*) two northern California debris flows, and (*d*) six Southwest debris flows. Larger 50% credible regions indicate greater uncertainty in the flow-mobility parameters. There was more uncertainty for the eight debris flows outside of Southern California than for the four southern California debris flows. Note the differences in scale in each panel.

local calibration site. The catalog of posterior distributions developed here can be sampled to support probabilistic forward model analyses of debris-flow runout (Aaron *et al.* 2022). However, both conventional and Bayesian calibration approaches demonstrate substantial site-to-site variability, even for debris flows within the same geographic region, suggesting that site-specific factors are more important for constraining flow-mobility parameters than regional-scale factors. This is particularly true for the debris flows in northern California and the Southwest for the reasons outlined below.

Regional controls

The variability in the optimal flow-mobility parameters and posterior distributions for debris flows in northern California and the Southwest may be partially attributed to the geologic and climatologic diversity of these regions. We grouped the 12 debris flows into broad geographic regions, mainly because the number of debris-flow inundation observations did not support partitioning the data into a greater number of more refined regions. These results, however, indicate that the chosen regions could be too broad to identify controls on the optimal flow-mobility parameters or posterior distributions, as sites within a region could still be separated by several hundred kilometers (Fig. 1). Thus, although there may be broad similarities in rainfall characteristics and geologic setting between sites in these regions, there are also substantial differences in dominant land cover, climate, sediment availability and local geology that could exert an equal or greater control on the optimal flow-mobility parameters. Given a larger set of debris-flow inundation

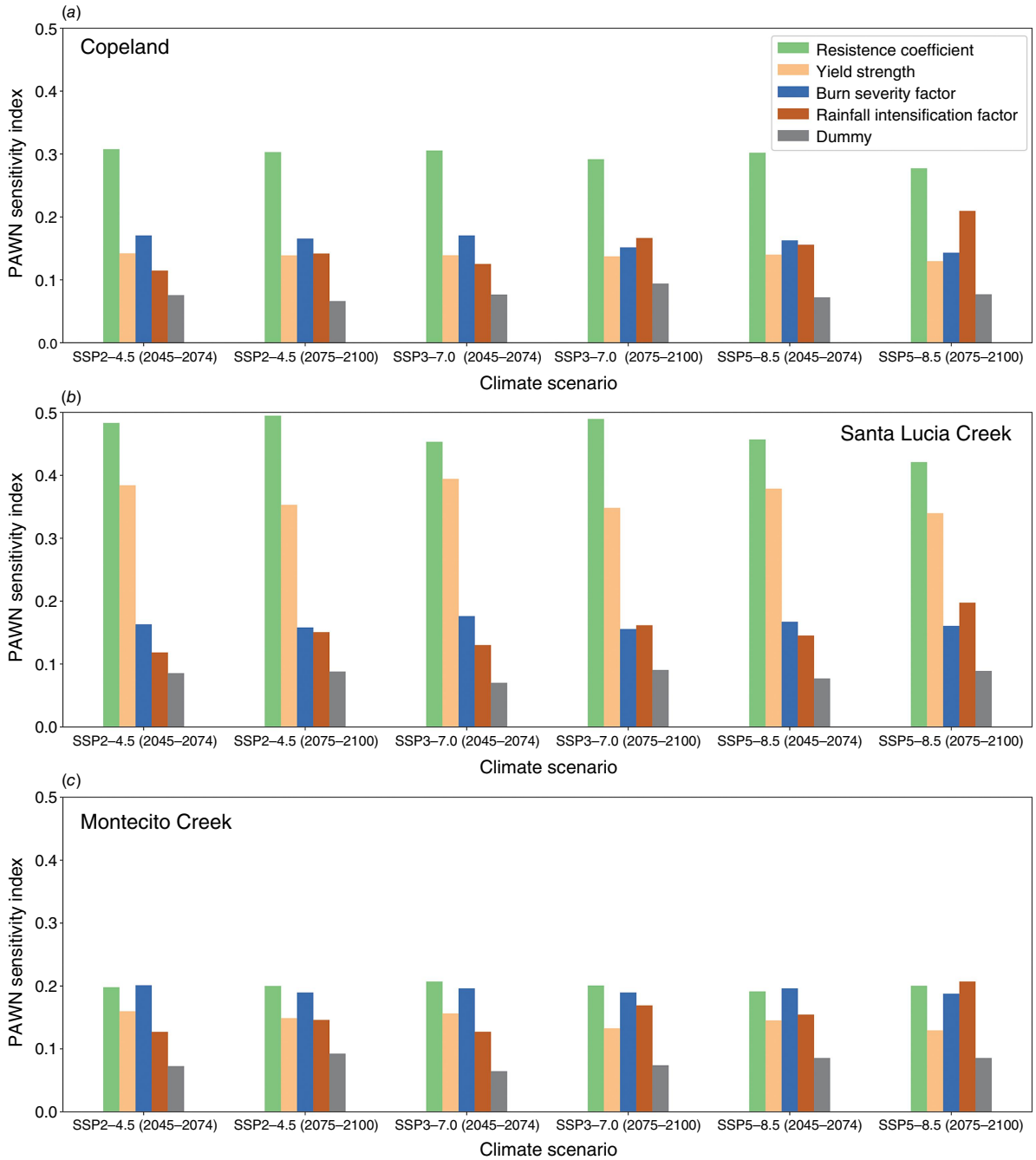

Fig. 5. Summary of the PAWN sensitivity analysis for the (*a*) Copeland, (*b*) Santa Lucia Creek, and (*c*) Montecito Creek study sites. A greater PAWN sensitivity index indicates that the modeled area inundated is more sensitive to the model parameter.

observations, future studies could examine the effects of these more local controls on flow-mobility parameters.

In contrast to the northern California and Southwest debris flows, the four southern California debris flows shared many similar characteristics. The Thomas Fire and Fish Fire debris flows occurred in the same Environmental Protection Agency (EPA) Level III ecoregion and Köppen–Geiger climate classification and had similar prefire land cover and underlying lithology. Perhaps owing to the close proximity and shared characteristics of the southern California sites, the optimal flow-mobility parameters and posterior distributions of the Southern California debris flows were more similar than those of the northern California or Southwest debris flows (Fig. 4).

Local controls

The strongest site-specific relationship we observed was the significant negative relationship between clay content and yield strength (τ) (Fig. 2). This relationship is supported by our understanding of how clay content influences pore-fluid pressure and debris-flow runout. The fine fraction of flows, which consists of silt and clay-sized grains, can help sustain high pore-fluid pressures that reduce frictional resistance and increase flow mobility (Iverson 1997). In simulations of ProDF, higher τ values yield less-mobile flows (Gorr *et al.* 2022), so the negative relationship between clay content and τ is consistent with the conceptual model that clay content increases retention of pore-fluid pressure and therefore increases debris-flow mobility. There is still substantial scatter in the data, however, including an outlier where the conventional calibration identified a yield strength for the Inyo Creek debris flow that lies well below the best fit line (Fig. 3*a*).

This relationship between clay content and τ can be used to inform forward analyses of debris-flow runout because clay content data are readily available for the entire United States. The STATSGO database (Schwarz and Alexander 1995) provides coarse-resolution data related to soil characteristics, including clay content, that can be incorporated into debris-flow runout frameworks. Although the relationship between clay content and τ was statistically significant for the debris flows in our dataset, the range of clay contents represented in the study watersheds was fairly narrow, spanning 7.5% (Inyo Complex) to 21.7% (Thomas Fire) (Table 2). Additional work is needed to evaluate the applicability of this relationship in scenarios with clay contents outside of this range. Additionally, we did not identify any significant relationships between either flow volume or clay content and the optimal flow resistance coefficient (χ). The variation in the site-to-site optimal χ value could be driven by a range of factors not accounted for here, including detailed information about the grain-size distribution of the flow, sediment concentration, and/or spatial and temporal variations in pore-fluid pressure.

Further constraining flow-mobility parameters

Future efforts to constrain flow-mobility parameters could benefit from debris-flow runout data that constrain factors beyond inundation extent, such as peak-flow velocity, flow depth, or flow timing. This information could reduce the variance of the posterior distributions and the size of the 50% credible regions. These data could be integrated into either the conventional or Bayesian calibration approach through the use of a multi-criteria objective function that quantifies the model's ability to reproduce the mapped inundation pattern as well as match observed velocity and/or flow depth estimates (Aaron *et al.* 2019; Gorr *et al.* 2024*b*). We observed a modest correlation between χ and τ, which can make it challenging to uniquely identify optimal parameter values because the effects of an increase in one parameter could be partially offset by a decrease in the other. Observations of flow depth and velocity could be particularly beneficial for placing additional constraints on χ, which directly influences modeled peak-flow depth and velocity. A multi-criteria objective function could also help constrain flow-mobility parameters for small flows, where uncertainty in the mapped inundation extent translated into greater uncertainty in the optimal flow-mobility parameters. Additional information about flow constituents, including sediment concentration and grain-size distribution, could also provide insight into factors controlling mobility parameters.

Implications for debris-flow hazard assessment

Estimates of debris-flow inundation are an important component of assessing debris-flow hazard and risk (McCoy *et al.* 2016). Many assessments of debris-flow hazards take place after a fire has already burned (e.g. Staley *et al.* 2016). These assessments have the benefit of information about burn severity, which affects modeled inundation zones through the influence of burn severity on flow volume (Gartner *et al.* 2014; Wall *et al.* 2023; Gorr *et al.* 2024*a*) and do not need to account for rainfall intensification that could occur in subsequent decades because the majority of PFDFs occur within the first several years following fire (McGuire *et al.* 2024). However, there can still be substantial uncertainty in the model parameters that affect flow mobility (Fig. 4). The posterior distributions developed here using the Bayesian calibration approach could be particularly useful for hazard assessment applications given the benefits of modeled inundation maps that reflect uncertainty (Barnhart *et al.* 2021).

Because the scope of post-fire debris-flow hazard assessments is often limited by the short time frame between fire occurrence and debris-flow initiation, prefire assessments of PFDF hazards can be used to develop and evaluate hazard mitigation plans (Tillery and Haas 2016; Fraser *et al.* 2022; Li and Chester 2023; Rossi *et al.* 2025), including fuel reduction treatments aimed at reducing the severity of future fires or improvements to infrastructure. As prefire assessments are completed in advance of a fire, burn severity and rainfall intensity–duration–frequency relationships are sources of uncertainty alongside the flow-mobility parameters. Results of the sensitivity analysis highlight the importance of having a calibration site for constraining flow-mobility parameters because χ had the highest relative importance in 15 of the 18 cases explored here (Fig. 5). The relative sensitivity to flow-mobility parameters is likely to increase when they take on values over a wider range, as might be prescribed based on expert judgment when there is no local calibration site. Although ProDF may be most sensitive to the flow-mobility parameters in many cases, it is also sensitive to the rainfall intensification factor (Fig. 5). As such, incorporating the effects of rainfall intensification in design storms (Martel *et al.* 2021) for prefire assessments

of PFDF hazards could be beneficial, especially in late-century scenarios. Additionally, although we focus primarily on the prefire assessment of post-fire hazards in this study, this framework could also be used to assess the impact of rainfall intensification on debris-flow hazards in unburned settings by utilizing a volume model that does not require information on burn severity (e.g. the V2 model in Gorr *et al.* 2024*a*).

Conclusions

As PFDFs become more prevalent in the western US, improved methods for hazard assessment are needed to help develop strategies for mitigating the impacts of future events. Runout modeling can be a key component of debris-flow hazard assessments. However, the lack of debris-flow runout data from recently burned areas has limited our ability to calibrate model parameters. Here, we used back-analyses of 12 runoff-generated debris flows, including 10 PFDFs, to constrain flow-mobility parameters for the Progressive Debris-Flow routing and inundation model. We used a conventional calibration technique to identify a single set of optimal flow-mobility parameters for each debris flow, as well as a Bayesian approach to identify a range of flow-mobility parameters that can be used in probabilistic predictions of debris-flow runout. We also assessed the sensitivity of modeled area inundated to variations in flow-mobility parameters, burn severity and rainfall intensification under future climate scenarios. Model calibration indicates that there is a negative, linear relationship between one of the flow-mobility parameters, debris-flow yield strength, and watershed soil clay content. Additionally, although the sensitivity analysis indicated that ProDF was most sensitive to the flow-mobility parameter values, the rainfall intensification factor was more influential than burn severity in late-century climate scenarios, revealing the benefit of considering rainfall intensification in future analyses. This work improves our ability to model debris-flow runout in prefire settings by reducing uncertainty in flow-mobility parameters and providing the foundation for a larger post-fire debris-flow runout database.

Supplementary material

Supplementary material is available online.

References

Aaron J, McDougall S, Nolde N (2019) Two methodologies to calibrate landslide runout models. *Landslides* **16**(5), 907–920. doi:10.1007/s10346-018-1116-8

Aaron J, McDougall S, Kowalski J, Mitchell A, Nolde N (2022) Probabilistic prediction of rock avalanche runout using a numerical model. *Landslides* **19**(12), 2853–2869. doi:10.1007/s10346-022-01939-y

Barnhart KR, Jones RP, George DL, McArdell BW, Rengers FK, Staley DM, Kean JW (2021) Multi-model comparison of computed debris flow runout for the 9 January 2018 Montecito, California post-wildfire event. *Journal of Geophysical Research: Earth Surface* **126**(12), e2021JF006245. doi:10.1029/2021JF006245

Conedera M, Peter L, Marxer P, Forster F, Rickenmann D, Re L (2003) Consequences of forest fires on the hydrogeological response of mountain catchments: a case study of the Riale Buffaga, Ticino, Switzerland. *Earth Surface Processes and Landforms* **28**(2), 117–129. doi:10.1002/esp.425

Corominas J (1996) The angle of reach as a mobility index for small and large landslides. *Canadian Geotechnical Journal* **33**(2), 260–271. doi:10.1139/t96-005

de Haas T, Braat L, Leuven JRFW, Lokhorst IR, Kleinhans MG (2015) Effects of debris flow composition on runout, depositional mechanisms, and deposit morphology in laboratory experiments. *Journal of Geophysical Research: Earth Surface* **120**(9), 1949–1972. doi:10.1002/2015JF003525

Esposito G, Gariano SL, Masi R, Alfano S, Giannatiempo G (2023) Rainfall conditions leading to runoff-initiated post-fire debris flows in Campania, Southern Italy. *Geomorphology* **423**, 108557. doi:10.1016/j.geomorph.2022.108557

Fowler HJ, Lenderink G, Prein AF, Westra S, Allan RP, Ban N, Barbero R, Berg P, Blenkinsop S, Do HX, Guerreiro S, Haerter JO, Kendon EJ, Lewis E, Schaer C, Sharma A, Villarini G, Wasko C, Zhang X (2021) Anthropogenic intensification of short-duration rainfall extremes. *Nature Reviews Earth & Environment* **2**(2), 107–122. doi:10.1038/s43017-020-00128-6

Fraser AM, Chester MV, Underwood BS (2022) Wildfire risk, post-fire debris flows, and transportation infrastructure vulnerability. *Sustainable and Resilient Infrastructure* **7**(3), 188–200. doi:10.1080/23789689.2020.1737785

García-Ruiz JM, Arnáez J, Gómez-Villar A, Ortigosa L, Lana-Renault N (2013) Fire-related debris flows in the Iberian Range, Spain. *Geomorphology* **196**, 221–230. doi:10.1016/j.geomorph.2012.03.032

Gartner JE, Cannon SH, Santi PM, Dewolfe VG (2008) Empirical models to predict the volumes of debris flows generated by recently burned basins in the western U.S. *Geomorphology* **96**(3), 339–354. doi:10.1016/j.geomorph.2007.02.033

Gartner JE, Cannon SH, Santi PM (2014) Empirical models for predicting volumes of sediment deposited by debris flows and sediment-laden floods in the transverse ranges of southern California. *Engineering Geology* **176**, 45–56. doi:10.1016/j.enggeo.2014.04.008

Gorr AN, McGuire LA, Youberg AM, Rengers FK (2022) A progressive flow-routing model for rapid assessment of debris-flow inundation. *Landslides* **19**(9), 2055–2073. doi:10.1007/s10346-022-01890-y

Gorr AN, McGuire LA, Beers R, Hoch OJ (2023) Triggering conditions, runout, and downstream impacts of debris flows following the 2021 Flag Fire, Arizona, USA. *Natural Hazards* **117**(3), 2473–2504. doi:10.1007/s11069-023-05952-9

Gorr A, McGuire L, Youberg A (2024*a*) Empirical Models for Postfire Debris-Flow Volume in the Southwest United States. *Journal of Geophysical Research: Earth Surface* **129**(11), e2024JF007825. doi:10.1029/2024JF007825

Gorr AN, McGuire LA, Youberg AM, Beers R, Liu T (2024*b*) Inundation and flow properties of a runoff-generated debris flow following successive high-severity wildfires in northern Arizona, USA. *Earth Surface Processes and Landforms* **49**(2), 622–641. doi:10.1002/esp.5724

Griffith GE, Omernik JM, Smith DW, Cook TD, Tallyn E, Moseley K, Johnson CB (2016) Ecoregions of California. 2016–1021. (US Geological Survey)

Griswold JP, Iverson RM (2008) Mobility statistics and automated hazard mapping for debris flows and rock avalanches. 2007-5276. (US Geological Survey)

Heiser M, Scheidl C, Kaitna R (2017) Evaluation concepts to compare observed and simulated deposition areas of mass movements. *Computational Geosciences* **21**(3), 335–343. doi:10.1007/s10596-016-9609-9

Hill RA, Weber MH, Leibowitz SG, Olsen AR, Thornbrugh DJ (2016) The Stream-Catchment (StreamCat) dataset: a database of watershed metrics for the conterminous United States. *JAWRA Journal of the American Water Resources Association* **52**(1), 120–128. doi:10.1111/1752-1688.12372

Hürlimann M, Rickenmann D, Medina V, Bateman A (2008) Evaluation of approaches to calculate debris-flow parameters for hazard assessment. *Engineering Geology* **102**(3), 152–163. doi:10.1016/j.enggeo.2008.03.012

Iverson RM (1997) The physics of debris flows. *Reviews of Geophysics* **35**(3), 245–296. doi:10.1029/97RG00426

Jin T, Hu X, Liu B, Xi C, He K, Cao X, Luo G, Han M, Ma G, Yang Y, Wang Y (2022) Susceptibility prediction of post-fire debris flows in Xichang, China, using a logistic regression model from a spatio-temporal perspective. *Remote Sensing* **14**(6), 1306. doi:10.3390/rs14061306

Kean JW, Staley DM (2021) Forecasting the frequency and magnitude of post-fire debris flows across southern California. *Earth's Future* **9**(3), e2020EF001735. doi:10.1029/2020EF001735

Kean JW, Staley DM, Cannon SH (2011) *In situ* measurements of post-fire debris flows in southern California: comparisons of the timing and magnitude of 24 debris-flow events with rainfall and soil moisture conditions. *Journal of Geophysical Research: Earth Surface* **116**(F4), F04019. doi:10.1029/2011JF002005

Kean JW, Staley DM, Lancaster JT, Rengers FK, Swanson BJ, Coe JA, Hernandez JL, Sigman AJ, Allstadt KE, Lindsay DN (2019) Inundation, flow dynamics, and damage in the 9 January 2018 Montecito debris-flow event, California, USA: opportunities and challenges for post-wildfire risk assessment. *Geosphere* **15**(4), 1140–1163. doi:10.1130/GES02048.1

Lamjiri MA, Dettinger MD, Ralph FM, Oakley NS, Rutz JJ (2018) Hourly analyses of the large storms and atmospheric rivers that provide most of California's precipitation in only 10 to 100 hours per year. *San Francisco Estuary and Watershed Science* **16**(4).

Li R, Chester MV (2023) Vulnerability of California roadways to post-wildfire debris flows. *Environmental Research: Infrastructure and Sustainability* **3**(1), 015003. doi:10.1088/2634-4505/acb3f5

Liu T, McGuire LA, Youberg AM, Prescott AB, Gorr AN, Struble WT, Beers R (2024) A prefire approach for probabilistic assessments of postfire debris-flow inundation. *Earth's Future* **12**(6), e2023EF004318. doi:10.1029/2023EF004318

Major JJ, Pierson TC (1992) Debris flow rheology: experimental analysis of fine-grained slurries. *Water Resources Research* **28**(3), 841–857. doi:10.1029/91WR02834

Martel J-L, Brissette FP, Lucas-Picher P, Troin M, Arsenault R (2021) Climate change and rainfall intensity–duration–frequency curves: overview of science and guidelines for adaptation. *Journal of Hydrologic Engineering* **26**(10), 03121001. doi:10.1061/(ASCE)HE.1943-5584.0002122

Martinez JR, McGuire LA, Youberg AM (2025) Insights into temporal changes in debris flow susceptibility following fire in the Southwest USA from monitoring and repeat estimates of soil hydraulic and physical properties. *Earth Surface Processes and Landforms* **50**(2), e70015. doi:10.1002/esp.70015

McCoy K, Krasko V, Santi P, Kaffine D, Rebennack S (2016) Minimizing economic impacts from post-fire debris flows in the western United States. *Natural Hazards* **83**(1), 149–176. doi:10.1007/s11069-016-2306-0

McGuire LA, Youberg AM, Rengers FK, Abramson NS, Ganesh I, Gorr AN, Hoch O, Johnson JC, Lamom P, Prescott AB, Zanetell J, Fenerty B (2021) Extreme precipitation across adjacent burned and unburned watersheds reveals impacts of low severity wildfire on debris-flow processes. *Journal of Geophysical Research: Earth Surface* **126**(4), e2020JF005997. doi:10.1029/2020JF005997

McGuire LA, Ebel BA, Rengers FK, Vieira DCS, Nyman P (2024) Fire effects on geomorphic processes. *Nature Reviews Earth & Environment* **5**(7), 486–503. doi:10.1038/s43017-024-00557-7

McKay MD, Beckman RJ, Conover WJ (1979) Comparison of three methods for selecting values of input variables in the analysis of output from a computer code. *Technometrics* **21**(2), 239–245. doi:10.1080/00401706.1979.10489755

Morelan A (2021) July 12, 2008 Oak Creek Debris Flow: Pre- and Post-Event DSM Creation and Vertical Differencing. (California Geological Survey Technical Report)

Nyman P, Sheridan GJ, Smith HG, Lane PNJ (2011) Evidence of debris flow occurrence after wildfire in upland catchments of south-east Australia. *Geomorphology* **125**(3), 383–401. doi:10.1016/j.geomorph.2010.10.016

Nyman P, Smith HG, Sherwin CB, Langhans C, Lane PNJ, Sheridan GJ (2015) Predicting sediment delivery from debris flows after wildfire. *Geomorphology* **250**, 173–186. doi:10.1016/j.geomorph.2015.08.023

Pianosi F, Wagener T (2015) A simple and efficient method for global sensitivity analysis based on cumulative distribution functions. *Environmental Modelling & Software* **67**, 1–11. doi:10.1016/j.envsoft.2015.01.004

Pierce DW, Cayan DR, Feldman DR, Risser MD (2023) Future increases in North American extreme precipitation in CMIP6 downscaled with LOCA. *Journal of Hydrometeorology* **24**, 951–975. doi:10.1175/JHM-D-22-0194.1

PRISM Climate Group (2025) [Dataset]. Oregon State University. Available at https://prism.oregonstate.edu

Radeloff VC, Helmers DP, Kramer HA, Mockrin MH, Alexandre PM, Bar-Massada A, Butsic V, Hawbaker TJ, Martinuzzi S, Syphard AD, Stewart SI (2018) Rapid growth of the US wildland–urban interface raises wildfire risk. *Proceedings of the National Academy of Sciences* **115**(13), 3314–3319. doi:10.1073/pnas.1718850115

Rickenmann D (1999) Empirical relationships for debris flows. *Natural Hazards* **19**(1), 47–77. doi:10.1023/A:1008064220727

Rossi RK, Richardson PW, Cavagnaro DB, Lukashov SG, Miller ME, Lindsay DN (2025) Predicting potential post-fire debris-flow hazards across California prior to wildfire. *International Journal of Wildland Fire* **34**(7), WF24225. doi:10.1071/WF24225

Schwarz GE, Alexander RB (1995) State Soil Geographic (STATSGO) Data Base for the Conterminous United States. U.S. Geological Survey Open-File Report. doi:10.3133/ofr95449

Senande-Rivera M, Insua-Costa D, Miguez-Macho G (2022) Spatial and temporal expansion of global wildland fire activity in response to climate change. *Nature Communications* **13**(1), 1208. doi:10.1038/s41467-022-28835-2

Sheppard PR, Comrie AC, Packin GD, Angersbach K, Hughes MK (2002) The climate of the US Southwest. *Climate Research* **21**(3), 219–238. doi:10.3354/cr021219

Skinner CJ (2016) Probability Proportional to Size (PPS) Sampling. In 'Wiley StatsRef: Statistics Reference Online'. (Eds N Balakrishnan, T Colton, B Everitt, W Piegorsch, F Ruggeri, JL Teugels) pp. 1–5. (John Wiley & Sons, Ltd)

Staley DM, Negri JA, Kean JW, Laber JL, Tillery AC, Youberg AM (2016) Updated logistic regression equations for the calculation of post-fire debris-flow likelihood in the western United States. 2016–1106. (US Geological Survey)

Staley DM, Tillery AC, Kean JW, McGuire LA, Pauling HE, Rengers FK, Smith JB (2018) Estimating post-fire debris-flow hazards prior to wildfire using a statistical analysis of historical distributions of fire severity from remote sensing data. *International Journal of Wildland Fire* **27**(9), 595–608. doi:10.1071/WF17122

Staley DM, Kean JW, Rengers FK (2020) The recurrence interval of post-fire debris-flow generating rainfall in the southwestern United States. *Geomorphology* **370**, 107392. doi:10.1016/j.geomorph.2020.107392

Thomas MA, Kean JW, McCoy SW, Lindsay DN, Kostelnik J, Cavagnaro DB, Rengers FK, East AE, Schwartz JY, Smith DP, Collins BD (2023) Postfire hydrologic response along the Central California (USA) coast: insights for the emergency assessment of postfire debris-flow hazards. *Landslides* **20**(11), 2421–2436. doi:10.1007/s10346-023-02106-7

Thomas MA, Michaelis AC, Oakley NS, Kean JW, Gensini VA, Ashley WS (2024) Rainfall intensification amplifies exposure of American Southwest to conditions that trigger postfire debris flows. *npj Natural Hazards* **1**(1), 14. doi:10.1038/s44304-024-00017-8

Tillery AC, Haas J (2016) Potential postwildfire debris-flow hazards - A prewildfire evaluation for the Jemez Mountains, north-central New Mexico. Scientific Investigations Report 2016-5101. 27 p. (US Department of the Interior, US Geological Survey: Reston, VA) doi:10.3133/sir20165101

Wall S, Murphy BP, Belmont P, Yocom L (2023) Predicting post-fire debris flow grain sizes and depositional volumes in the Intermountain West, United States. *Earth Surface Processes and Landforms* **48**(1), 179–197. doi:10.1002/esp.5480

Wells AG, Hawbaker TJ, Hiers JK, Kean J, Loehman RA, Steblein PF (2023) Predicting burn severity for integration with post-fire debris-flow hazard assessment: a case study from the Upper Colorado River

Basin, USA. *International Journal of Wildland Fire* **32**(9), 1315–1331. doi:10.1071/WF22200
Whipple KX, Dunne T (1992) The influence of debris-flow rheology on fan morphology, Owens Valley, California. *GSA Bulletin* **104**(7), 887–900. doi:10.1130/0016-7606(1992)104<0887:TIODFR>2.3.CO;2
Wilken E, Nava FJ, Griffith G (2011) North American Terrestrial Ecoregions - Level III. Commission for Environmental Cooperation. (Montreal, Canada)
Youberg, AM (2015) Geodatabase of Post-Wildfire Study Basins: assessing the predictive strengths of post-wildfire debris-flow models in Arizona and defining rainfall intensity-duration thresholds for initiation of post-fire debris flows [Dataset]. Arizona Geological Survey. Available at https://library.azgs.arizona.edu/item/AGDI-1552428145135-106
Zimmermann F, McArdell BW, Rickli C, Scheidl C (2020) 2D Runout modelling of hillslope debris flows, based on well-documented events in Switzerland. *Geosciences* **10**(2), 70. doi:10.3390/geosciences1002007

Data availability. ProDF was coded in C and utilized MATLAB scripts to write input files and read output files. Code for the numerical model (ProDF) is located at https://www.hydroshare.org/resource/c45c7c602b9746da9e8ff99bd94b0676/.

Conflicts of interest. Authors Luke McGuire and Ann Youberg are Guest Editors of *International Journal of Wildland Fire* but were not involved in the peer review or decision-making process for this paper. The authors have no further conflicts of interest to declare.

Declaration of funding. This work was supported by the California Department of Water Resources Atmospheric River Program (4600013361), the US Geological Survey under Grant/Cooperative Agreement No. G23AC00447-00 and a JFSP GRIN awarded to Alexander Gorr (23-1-01-28).

Acknowledgements. We thank Scott McCoy for sharing debris flow inundation and volume data for the Dolan Fire and Tamarack Fire sites.

Author affiliations
[A]The University of Arizona, Department of Geosciences, Gould-Simpson Building, 1040 East Fourth Street, Tucson, AZ 85721, USA.
[B]The University of Arizona, Arizona Geological Survey, 1955 E 6th Street, Tucson, AZ 85721, USA.
[C]California Geological Survey, 6105 Airport Road, Redding, CA 96002, USA.